Dynamic disulfide exchange in a crystallin protein in the human eye lens promotes cataract-associated aggregation

Received for publication, June 21, 2018, and in revised form, September 14, 2018 Published, Papers in Press, September 21, 2018, DOI 10.1074/jbc.RA118.004551

Eugene Serebryany[‡], Shuhuai Yu[§], Sunia A. Trauger[¶], Bogdan Budnik[‖], and Eugene I. Shakhnovich[‡1]

From the [‡]Department of Chemistry and Chemical Biology, Harvard University, Cambridge, Massachusetts 02138, [§]State Key Laboratory of Food Science and Technology, Jiangnan University, Wuxi, 214122 Jiangsu, China, and [¶]Small Molecule Mass Spectrometry Core Facility and [‖]Mass Spectrometry and Proteomics Resource Laboratory, Faculty of Arts and Sciences, Harvard University, Cambridge, Massachusetts 02138

Edited by Velia M. Fowler

Increased light scattering in the eye lens due to aggregation of the long-lived lens proteins, crystallins, is the cause of cataract disease. Several mutations in the gene encoding human γD-crystallin (HγD) cause misfolding and aggregation. Cataract-associated substitutions at Trp^{42} cause the protein to aggregate *in vitro* from a partially unfolded intermediate locked by an internal disulfide bridge, and proteomic evidence suggests a similar aggregation precursor is involved in age-onset cataract. Surprisingly, WT HγD can promote aggregation of the W42Q variant while itself remaining soluble. Here, a search for a biochemical mechanism for this interaction has revealed a previously unknown oxidoreductase activity in HγD. Using *in vitro* oxidation, mutational analysis, cysteine labeling, and MS, we have assigned this activity to a redox-active internal disulfide bond that is dynamically exchanged among HγD molecules. The W42Q variant acts as a disulfide sink, reducing oxidized WT and forming a distinct internal disulfide that kinetically traps the aggregation-prone intermediate. Our findings suggest a redox "hot potato" competition among WT and mutant or modified polypeptides wherein variants with the lowest kinetic stability are trapped in aggregation-prone intermediate states upon accepting disulfides from more stable variants. Such reactions may occur in other long-lived proteins that function in oxidizing environments. In these cases, aggregation may be forestalled by inhibiting disulfide flow toward mutant or damaged polypeptides.

In vivo populations of many proteins exhibit conformational and chemical heterogeneity (1–8). This heterogeneity may arise from post-translational modifications, somatic mutations, or roughness of the conformational landscape or simply as a natural effect of heterozygosity. Biochemical heterogeneity is particularly important for highly abundant, long-lived (low-turnover) proteins, such as the collagens and aggrecans of the joints; elastins of the skin; and crystallins of the eye, which accumulate damage throughout the course of life (9–11). For well structured proteins, partially populated intermediate and misfolded conformational states give rise to heterogeneous conformational ensembles in living cells, which sometimes leads to aggregation (12–15). The emergent properties of subtly heterogeneous macromolecular populations are largely unexplored, yet there is ample evidence that they can be significant (1, 4, 16). Perhaps the most spectacular case is the prion effect wherein polypeptides in an aggregation-prone conformational state can catalyze conformational conversion and aggregation in the natively folded polypeptides (17). Specific mutations or post-translational modifications can enhance or suppress these aggregation-promoting interactions, *e.g.* in the ALS-associated enzyme superoxide dismutase 1 (18); in β_2-microglobulin, associated with dialysis amyloidosis (19); and in the yeast prion Sup35 (20).

Intramolecular disulfides are crucial for the correct folding of many proteins that function in relatively oxidizing environments, such as antibodies and hormones in the blood, transmembrane proteins, and digestive enzymes as well as a wide variety of protein toxins (21–27). At the same time, internal disulfides are well known conformational traps on the protein folding landscape, capable of stabilizing both productive folding intermediates and aggregation-prone misfolded states (28–32). Redox chemistry is known to be crucial for many proteins' aggregation pathways. These include superoxide dismutase 1, associated with ALS (31), as well as β_2-microglobulin, the amyloid-forming protein in dialysis amyloidosis (33, 34). Disulfide scrambling is an important failure mode of therapeutic antibodies (21) and may be involved in light-chain amyloidosis (35). Domain swapping is a particularly sensible mechanism for aggregation via disulfide-stabilized intermediate states, and indeed this may play a role in serpinopathies (36). Dynamic disulfide exchange among identical or nearly identical polypeptides has only been recently recognized, in the case of protein-disulfide isomerase (37), and is likely to be found in other systems. Most known proteins are capable of undergoing some reversible post-translational modifications, including a wide variety of disulfide bonds (1, 4, 38). Redox potential in various tissues changes over time in the course of development or across the cell cycle, due to episodes of oxidative stress, or in the course of aging (39–41).

This work was supported by the National Institutes of Health Grants R01GM111955 (to E. I. S.) and F32GM126651 (to E. S.). The authors declare that they have no conflicts of interest with the contents of this article. The content is solely the responsibility of the authors and does not necessarily represent the official views of the National Institutes of Health.
This article was selected as one of our Editors' Picks.
This article contains Figs. S2, S3, S5, and S6 and Tables S1 and S4.
[1] To whom correspondence should be addressed: Dept. of Chemistry and Chemical Biology, Harvard University, 12 Oxford St., Cambridge, MA 02138. Tel.: 617-495-4130; E-mail: shakhnovich@chemistry.harvard.edu.

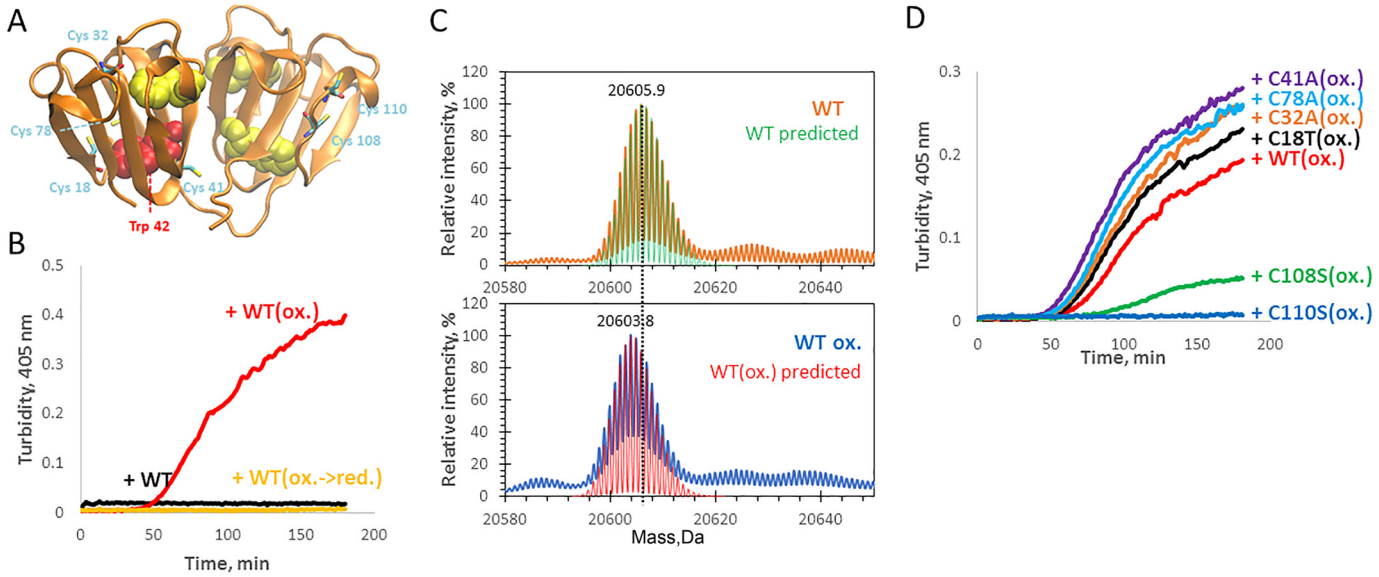

Figure 1. WT HγD can be toggled between the inert and aggregation-promoting states *in vitro* by formation or reduction of the 108–SS–110 internal disulfide bond. *A*, representation of the WT crystal structure in orthosteric projection (Protein Data Bank (PDB) code 1HK0) showing the location of the 6 Cys residues as well as Trp[42]. *B*, turbidity traces from mixtures of reduced W42Q with reduced (*black*), oxidized (*red*), and oxidized and re-reduced WT (*yellow*). The concentration of each protein was 50 μM. *C*, whole-protein isotopically resolved mass spectra showing WT(ox.) to be 2 Da lighter than the reduced version, indicating formation of one internal disulfide bond per molecule. Theoretical isotopically resolved mass spectra based solely on the atomic composition (*green* and *red*) are overlaid on the respective experimentally determined deconvoluted isotopically resolved mass spectra (*orange* and *blue*). *D*, WT HγD and variants at every Cys position were oxidized in parallel, and their ability to catalyze W42Q aggregation was tested (each protein at 50 μM). Resulting turbidity traces confirmed Cys[108] and Cys[110] as the residues predominantly responsible for the aggregation-promoting activity.

The eye lens is a remarkable study in proteome aging because the proteins in its core are never replaced. Their eventual misfolding and aggregation leads to cataract disease, lens opacification due to light scattering by the protein aggregates (42). Crystallins in the lens core are highly stable and soluble, resisting any long-range packing interactions, including formation of both native (crystals) and nonnative (amyloid or amorphous) aggregates (43). However, they accumulate damage over time, such as Cys and Trp oxidation as well as deamidation, truncation, and other changes (44–47). One of the most readily formed yet most consequential post-translational modifications that accumulate with aging is formation of disulfide bonds. Cells of the human eye lens core lack nuclei or organelles and are metabolically quiescent (48, 49), so their cytoplasm gets more oxidizing over time (50). Due to this lack of active metabolism, neither the redox enzymes nor the crystallins, which make up the bulk of the lens proteome, turn over (51, 52). The result is progressively higher disulfide content in lens crystallins during aging (51, 53–56). Oxidation of specific Cys residues to disulfides in lens crystallins correlates with the onset and progression of cataract disease (57–60).

GSH, which acts as the redox buffer in young lens, becomes depleted from the lens with age (50, 61, 62). Reduced and oxidized forms of GSH are both depleted, whereas protein and mixed disulfides increase (58, 63, 64). In fact, the concentration of GSH in aged and especially cataractous lenses is 0.2–2 mM (50, 63); crystallins are present in lens nuclei at up to 400 mg/ml (48), and γ-crystallins account for 20–25% of this total (65, 66), or ~4–5 mM, with 5–7 Cys residues each (depending on the type). This raises the possibility that even the redox buffering functions are transferred to the lens proteome during aging and cataractogenesis. The W42Q mutation mimics oxidative damage to Trp side chains (conversion to kynurenine, which is more hydrophilic) that is known to arise during aging (44, 47, 67); the W42R variant, whose biophysical properties are highly similar, causes hereditary cataract in humans (32, 68–70). We report that WT HγD[2] is able to act as an oxidoreductase, oxidizing the W42Q variant in a way that triggers its aggregation. Specifically, a pair of Cys residues in the C-terminal domain of HγD is capable of forming a labile disulfide bond. These disulfides are dynamically exchanged among crystallin molecules under physiological conditions in solution, creating a "redox hot potato" competition: the disulfide is passed around until it is transferred to a destabilized variant where it can lock the aggregation-prone intermediate; the ensuing aggregation removes both the destabilized variant and the disulfide from solution.

Results

WT HγD crystallin must be oxidized to promote aggregation of the W42Q mutant

We have reported previously (71) the surprising interaction between WT HγD crystallin and its cataract-associated W42Q mutant whereby the WT protein promoted the mutant's aggregation in a temperature- and concentration-dependent manner without aggregating itself. Formation of an internal disulfide bond was crucial for the mutant protein's ability to aggregate (32). Therefore, we explored the possibility that redox chemistry is involved in this aggregation-promoting mechanism.

We found that fully reduced purified WT protein had no activity with respect to W42Q aggregation. However, it could

[2] The abbreviations used are: HγD, human γD-crystallin; ox., oxidized; ESI, electrospray ionization; CCC, C18T/C41A/C78A; DSF, differential scanning fluorometry; HCD, high-energy collision dissociation.

be converted to an active form *in vitro* (Fig. 1*B*) by a commonly used oxidizing treatment with a 1:3 mixture of Cu(II) and phenanthroline (72, 73). After removing the oxidant by extensive dialysis, the WT(ox.) protein efficiently promoted aggregation of W42Q; reduction of WT(ox.) with tris(2-carboxyethyl)phosphine inactivated it again (Fig. 1*B*). Isotopically resolved whole-protein electrospray MS confirmed that the peak isotope mass of the WT sample prior to oxidation was 20,605.9 Da, which precisely matches the peak isotope mass predicted from the amino acid sequence (20,605.8 Da), and the overlap of isotopic distributions was also nearly perfect between the theoretical and experimentally determined mass spectra (Fig. 1*C*). The same experiment was carried out on the WT(ox.) sample whose activity was assayed in Fig. 1*B*, and the resulting molecular weight and isotope distribution both precisely matched those predicted for the protein in the case of one intramolecular disulfide bond per polypeptide (–SH + –SH → –S–S–; hence the loss of 2 Da) following the oxidizing treatment. Thus, the oxidation was highly specific, leaving the remaining 4 Cys residues unaffected, and essentially quantitative under these conditions.

A specific disulfide bond in the WT protein enables W42Q aggregation

The native-state crystal structure of HγD (Fig. 1*A*) has no disulfide bonds despite the statistically high proportion of Cys residues in this protein (6 of 173 residues). Tissue proteomic studies have revealed disulfide formation in this protein in the oxidizing cytosol of aged and cataractous lenses (58, 74). At least two pairs of Cys residues (18-78 and 108-110) are sufficiently close in the native structure that a disulfide bond might form with only a short-range structural perturbation. Other disulfides have been observed following mutation or denaturation of the protein (32, 74).

We therefore used site-directed mutagenesis to eliminate, one at a time, each of the 6 Cys residues on the WT background. Simultaneous oxidation of WT and Cys-mutant proteins under identical conditions showed no declines in aggregation-promoting activity, relative to WT, for any mutants except C108S and C110S, which lost all or most of this activity (Fig. 1*D*). Thus, the 108–SS–110 disulfide appeared to be crucial for the aggregation-promoting activity. We were able to directly detect this disulfide in LC-MS/MS spectra of chymotryptic digests of the oxidized protein (Table S1 and Fig. S2). This was additionally confirmed by top-down proteomics with incomplete chymotrypsin/Glu-C digestion, which yielded a peak at 10,382.4101 Da (consistent with residues 65–150 with one disulfide), which fragmented to yield a peak at 6921.9584 Da (consistent with residues 93–145 with 108–SS–110 as no other Cys residues are present between these positions). By contrast, combined tryptic/chymotryptic digests revealed that the N-terminal Cys residues (particularly Cys^{18} and Cys^{78}) were mostly in the reduced state (Table S1). A smaller amount of Cys^{18}-Cys^{32} disulfides was observed, although detection of Cys^{32}- and Cys^{41}-containing peptides proved challenging, in line with previous proteomic data (45).

Notably, isotopically resolved MS of the C108S and C110S variants following oxidative treatment revealed significant fractions of each variant with a rightward mass shift (Fig. S3), possibly due to oxidation of a His side chain. Thus, in our experiments the 108–SS–110 bond in HγD appeared to act as a preferred oxidation scavenger site to avoid irreversible oxidation of other residues. Furthermore, the C108S/C110S double mutant exhibited much less of the heavier species (Fig. S3), suggesting that this form of covalent damage was cysteine-mediated in some way.

Disulfide transfer from WT to W42Q promotes W42Q aggregation

We next tested whether this newly discovered oxidoreductase activity was related to the aggregation-promoting activity of the WT protein. This was accomplished by incubating a 1:1 mixture of oxidized WT and reduced W42Q until it turned turbid, indicating insolubilization of some fraction of the latter. Then, fresh W42Q was added, and the reaction was repeated for a total of four cycles, so that by the end the total amount of W42Q added was roughly 4× WT. By the fourth cycle, turbidity was visibly lower than initially. After each step, the turbid solution was centrifuged, and the pelleted fractions were washed, resuspended in sample buffer, and combined.

Whole-protein isotopically resolved ESI-TOF (Fig. 2) revealed that the supernatant at the end of the fourth aggregation cycle contained predominantly reduced WT protein and reduced W42Q. Thus, most of the disulfide-containing WT protein had been converted to the reduced form. Analysis of the pelleted fraction proved more difficult because the proteins were in an aggregated state. The aggregates were partially resolubilized in low-pH buffer (pH 5 ammonium acetate). ESI-TOF of this resolubilized protein revealed that it consisted predominantly of W42Q with one disulfide bond (−2-Da mass shift), consistent with our initial observations (71). It follows that oxidized WT HγD promoted W42Q aggregation by transferring a disulfide to it. The result can be summarized as a chemical reaction where the reactants WT(ox.) and W42Q are both soluble, whereas the products are soluble WT and insoluble W42Q(ox.). Aggregation of the oxidized mutant may shift the equilibrium in favor of disulfide transfer to the mutant.

The ability of W42Q to accept a disulfide bond and aggregate depended on the nature of the oxidant disulfide. Thus, GSH disulfide (GSSG) caused strong aggregation of W42Q with kinetics comparable with those observed upon addition of the oxidized WT protein. By contrast, the same amount of hen egg lysozyme had no effect on W42Q (Fig. 3*A*) despite the fact that lysozyme contains four disulfide bonds per molecule. We interpret the difference as arising from the much higher accessibility and/or redox potential of both the reversible Cys^{108}-Cys^{110} disulfide in WT HγD and the GSSG disulfide as compared with the structural disulfides in lysozyme. It is worth noting that disulfide geometry has a strong effect on whether it is a catalytic or a structural bond (38) and that the close sequence proximity of Cys^{108} and Cys^{110} is likely to give it a strained, catalytic-like configuration (24, 38, 75).

Because Trp oxidation is a relatively rare event in the lens, the concentration of species mimicked by the W42Q substitution is expected to be relatively low compared with WT. Therefore, we also carried out aggregation experiments in a different concen-

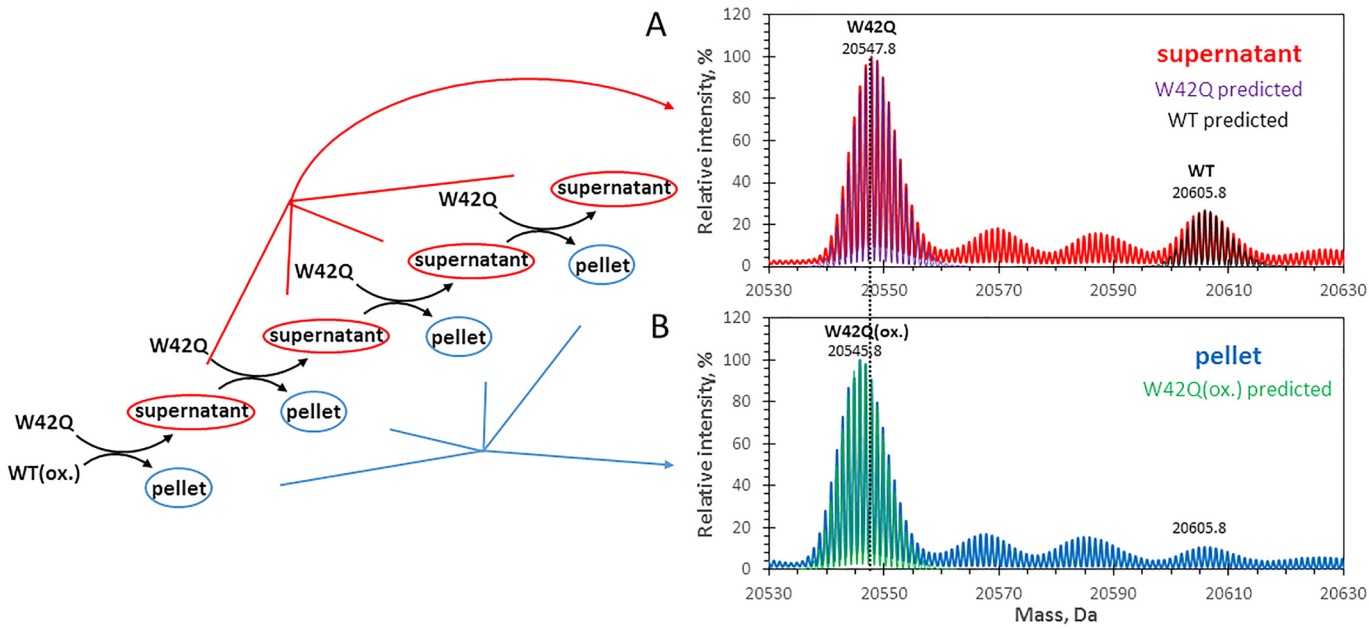

Figure 2. Disulfide transfer from soluble WT(ox.) to soluble W42Q generates soluble WT and aggregated W42Q(ox.). Whole-protein isotopically resolved mass spectra for the supernatant (*A*) and pelleted precipitate (*B*) fractions from aggregation mixtures of WT(ox.) with W42Q are shown. As shown in the schematic (*left*), W42Q was added at each step, but WT(ox.) was only added initially; hence, the total final [W42Q] in the experiment was 4 times the initial [WT(ox.)]. The pooled supernatant fractions (*A*) clearly contained only reduced W42Q as evidenced by the exact match between the observed (*red*; 20547.8 Da) and theoretically predicted (*purple*) isotope distributions, and the WT(ox.) sample had been almost completely reduced back to WT because the observed peak (*red*; 20,605.8 Da) skewed only slightly to the left compared with the theoretically predicted isotope distribution for the fully reduced WT (*black*). The pooled pelleted fractions contained exclusively −2-Da shifted W42Q as evidenced by the exact overlap between the experimental data (*blue*; 20,545.8 Da) and theoretically predicted isotope distribution for W42Q with one internal disulfide per molecule (*green*). Hence, the internal disulfide was transferred from soluble, oxidized WT to the soluble, reduced W42Q during the reaction, leading to formation of insoluble, oxidized W42Q.

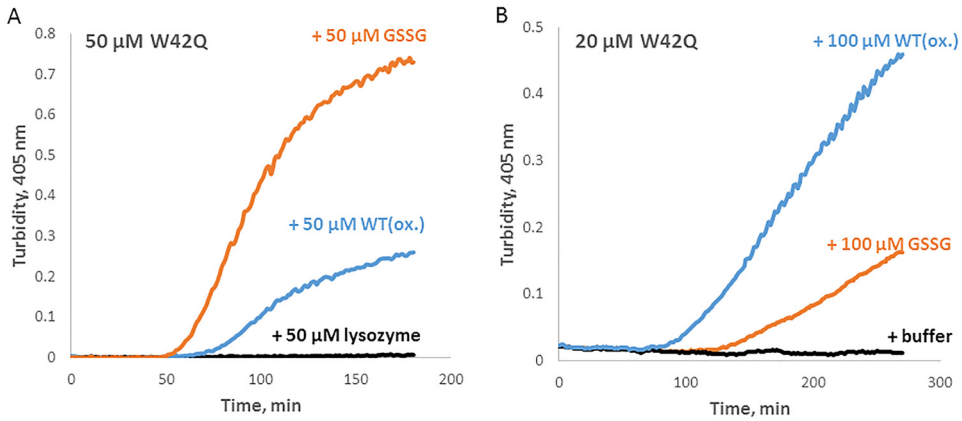

Figure 3. W42Q aggregation depends on dynamic nature of the oxidant disulfide. *A*, 50 μM W42Q protein was incubated at 37 °C and pH 7 in the presence of 50 μM hen egg lysozyme (*black*), 50 μM WT(ox.) (*blue*), or 50 μM oxidized GSH (*orange*). The four disulfide bonds per molecule in lysozyme are not dynamic in contrast to the single disulfide per molecule of oxidized WT or oxidized GSH. *B*, the relative aggregation-promoting abilities of GSSG and WT(ox.) are reversed in a distinct concentration regime (20 μM W42Q and 100 μM oxidant).

tration regime: 20 μM W42Q and 100 μM WT(ox.) or GSSG. Surprisingly, the relative aggregation-promoting abilities of GSSG and WT(ox.) were reversed in this concentration range, as shown in the representative traces in Fig. 3*B*. The reason WT(ox.) appears to be a weaker aggregation inducer than GSSG when [W42Q] is high but a stronger aggregation inducer when [W42Q] is low is the subject of ongoing investigation. As the pool of GSH becomes depleted in the lens with age, [WT(ox.)] is expected to increase, and the protein disulfides are likely to play a bigger role in promoting aggregation of damaged HγD polypeptides.

The disulfide required for W42Q aggregation was distinct from the dynamic 108–SS–110 disulfide in WT. LC-MS/MS (Table S4) revealed the internal disulfide in the W42Q aggregates to be predominantly 32–SS–41, consistent with previous results (32) as well as tissue proteomic analysis (58). However, given the importance of the 108–SS–110 bond in the WT(ox.) protein, we examined whether the same bond in the mutant affected its aggregation. The W42Q/C110S double mutant aggregated comparably with W42Q at neutral pH when mixed with the WT(ox.) protein but less so at lower pH (Fig. S5A). The ability to form the 108–SS–110 disulfide, however, appeared to confer modest aggregation resistance at lower concentrations of the oxidizing agent GSSG, perhaps because this site acted as an oxidation decoy, reducing or delaying oxidation of the N-terminal domain (Fig. S5*B*). Despite similarity at neutral pH,

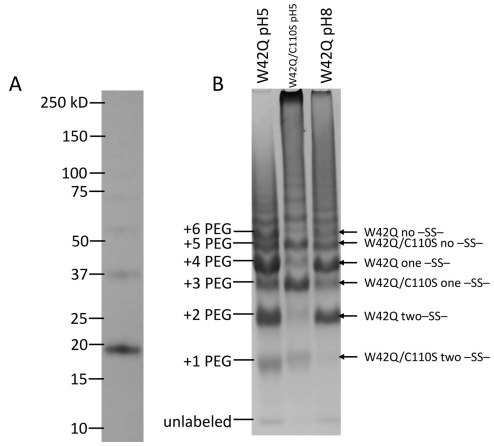

Figure 4. Distribution of disulfides in aggregated W42Q and W42Q/C110S by PEGylation. *A*, the SDS-resolubilized aggregates of W42Q were predominantly monomeric by nonreducing SDS-PAGE with only minor bands consistent with disulfide-cross-linked dimers and trimers visible on the gel. *B*, most aggregated monomers contained one internal disulfide with a smaller fraction containing two by PEGylation. *Left lane*, W42Q was mixed with oxidized WT, at increased concentration (75 μM each protein) at pH 5.5, to generate aggregates while minimizing disulfide scrambling, and distributions of the number of free –SH groups per molecule in SDS-resolubilized aggregates were quantified by PEG-maleimide. The major band was found at +4 PEG (of 6 Cys/molecule), indicating one internal disulfide per molecule, with a minor band at +2 PEG (two internal disulfides). *Middle lane*, the same was done for W42Q/C110S aggregates produced by mixing with oxidized C18T/C41A/C78A (75 μM each protein) at pH 5.5. The triple-Cys mutant was used to ensure that any contamination from the non-W42Q proteins in the aggregates could be easily seen by SDS-PAGE upon PEGylation (as +1 or +3 bands in the *W42Q lanes* and +4 or +6 bands in the *W42Q/C110S lane*, respectively). The predominant band for resolubilized monomers was at +3 PEG (of 5 Cys/molecule), indicating one internal bond per molecule. Lack of a prominent minor band at +1 PEG indicated that monomers with two internal disulfides were extremely rare. *Right lane*, for comparison, the same was done for W42Q mixed with oxidized WT (40 μM each protein) at pH 8 with results very similar to those obtained at pH 5.5. Because substantial numbers of monomers with two internal disulfides were found in W42Q aggregates but not W42Q/C110S aggregates, we attribute the second disulfide to 108–SS–110.

lower pH (pH 5) led to dramatically different behavior for the W42Q and W42Q/C110S variants. When mixed with the oxidizing agent Cu(II)/phenanthroline, only the single mutant aggregated at pH 5, whereas both did so at pH 7 (Fig. S5*C*). This difference suggests that Cys^{110} may retain its reactivity even at reduced pH; however, the mechanism of aggregation, including any potential intramolecular disulfide transfer, under these conditions remains to be investigated. Formation of 108–SS–110 in the mutant may promote formation of the N-terminal disulfide there under low pH conditions.

To gain quantitative understanding of the distribution of the number of free thiol groups per molecule, we also resolubilized aggregates in 5% SDS at 95 °C, pH 5, and used a PEGylation gel-shift assay similar to those reported previously (76–78). Free thiol groups reacting with maleimide-conjugated polyethylene glycol (PEG) generated predictable upshifts in migration through an SDS-polyacrylamide gel. PEGylation of free thiols in the aggregated state (Fig. 4) revealed that W42Q/C110S aggregates lost two free thiols per molecule, consistent with formation of one internal disulfide bond. The W42Q aggregates contained a major one-disulfide population and a minor, but still significant, population of molecules with two internal disulfide bonds. We infer that one of those bonds is 108–SS–110 and that its formation in the mutant is not required for aggregation.

The precise mechanism of W42Q misfolding and the precise extent of disordering of its N-terminal domain prior to 32–SS–41 formation remains to be investigated. The T_m for the first unfolding transition, corresponding to unfolding of the mutated N-terminal domain, is 55 °C (32). The domain contains 83 residues. Robertson and Murphy (79) reported average ΔH and ΔS values per residue at 60 °C for a large set of proteins (see Figs. 5*A* and 6*A* of Ref. 79). Using these values and assuming two-state unfolding of the W42Q N-terminal domain, we arrive at a predicted $\Delta G_{\text{unfolding}}$ of ~4 kcal/mol at 37 °C, or unfolding probability of $\sim 2 \times 10^{-3}$. Conversely, the W42Q variant contains the full complement of 6 Cys residues and hence could theoretically form any of 14 internal disulfides besides 108–SS–110. However, only one of those disulfides, 32–SS–41, has been found in W42Q aggregates in this study, consistent with the prior report that used a different experimental procedure (32). No detectable amount of disulfide was found in the soluble fraction of W42Q (Fig. 2*A*). This suggests the misfolding reaction leading to 32–SS–41 has a degree of specificity; it is likely to proceed through an intermediate with only a partially unfolded N-terminal domain.

Oxidoreductase activity of HγD enables dynamic disulfide exchange among soluble HγD variants

The reversible Cys^{108}-Cys^{110} disulfide of HγD bears similarity to the "*CXC*" motif of some thioredoxins and disulfide isomerases as well as the redox-switchable chaperone Hsp33 (75, 80, 81), so this γ-crystallin may have a previously unrecognized oxidoreductase function. The Cys^{110} thiol group is solvent-accessible in the native structure (82), suggesting that disulfide interchange among HγD molecules may occur in solution. It was recently reported (37) that some protein-disulfide isomerases are capable of dynamically exchanging disulfide bonds in solution, essentially forming a proteinaceous redox buffer in the endoplasmic reticulum. Given the high abundance of HγD in the lens core (up to ~10 mg/ml), it could potentially act as a supplementary redox buffer as GSH levels are depleted with age.

To explore this possibility, we incubated mixtures of HγD variants where one variant (or WT) started out as fully oxidized at the 108-110 site and the other started with those two residues fully reduced. The typical pK_a of a Cys residue is ~8. Therefore, incubations were carried out either at pH 8 (permissive for thiol-disulfide interchange) or at pH 5 (inhibiting interchange). Disulfide transfer was determined by quantifying the distributions of the number of free thiols per molecule for each of the variants at the end of the incubation via the PEGylation/gel-shift assay. As shown in Fig. 5, when reduced WT protein was incubated with the oxidized triple mutant C18T/C41A/C78A (abbreviated CCC) at pH 5, the vast majority of each respective polypeptide population was found at the migration positions expected for no disulfide exchange: the WT protein retained six free thiols per molecule (hence the prominent 6xPEG band), whereas the oxidized triple mutant had only one free thiol per molecule (hence the 1xPEG band). The band at 2xPEG was likely due to incomplete reaction between the CCC construct and the labeling reagent. The corresponding incubation mixture at pH 8 showed a significant decrease in the amount of

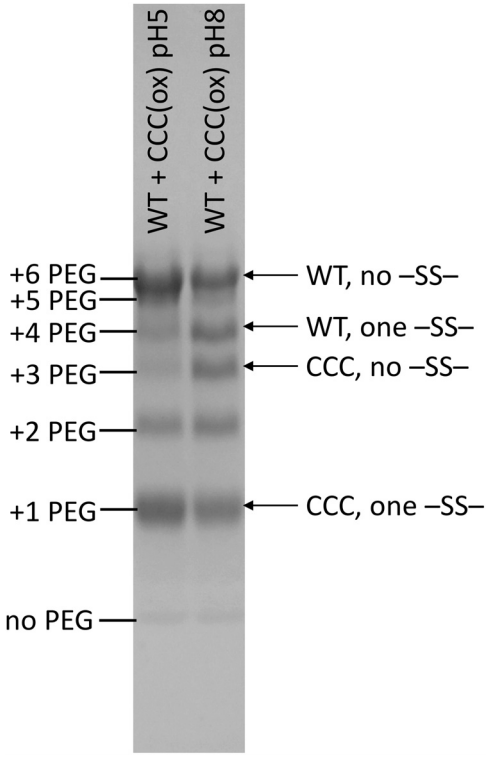

Figure 5. Evidence of disulfide transfer among soluble HγD molecules. An SDS-PAGE gel of samples incubated with maleimide-PEG to quantify the distribution of the number of free thiol groups per protein molecule is shown. When reduced WT protein was mixed with CCC(ox.) and incubated for 1 h at pH 5, at which disulfide exchange is inhibited (*left lane*), the resulting molecular population at the end of the reaction consisted largely of 6- and 1-free-thiol populations, corresponding to the starting samples. When pH in the same mixture was set to 8, allowing disulfide exchange (*right lane*), after 1 h the population shifted toward 4- and 3-free-thiol positions, corresponding to oxidized WT and reduced C18T/C41A/C78A, respectively.

6xPEG (WT) and 1xPEG (CCC(ox.)) bands and a concomitant increase in the 3xPEG and 4xPEG bands, attributable to formation of reduced CCC mutant and oxidized WT, respectively.

Formation of the 108–SS–110 disulfide conformationally strains the C-terminal domain

As we have demonstrated previously (32), oxidative aggregation of W42Q/R mutants proceeds at temperatures ~10 °C below the onset of any detectable unfolding of the N-terminal domain. However, it is clear by inspection that formation of the 108–SS–110 disulfide should introduce strain into the native structure. Most thioredoxin-type motifs are "C*XX*C" where *XX* are often Pro and Gly to enable the tight turn required to form the disulfide. In cases where C*X*C motifs are found, *X* is typically Gly (75, 80) because its range of backbone angles is the broadest. We therefore hypothesized that the CSC motif found here was likely to be strained, which accounts for the ease of disulfide exchange but may also contribute to conformational strain in the protein, potentially leading to partial unfolding.

To test this prediction experimentally, we studied both WT and the library of single- and multiple-Cys mutants in the WT background to determine whether 108–SS–110 formation indeed strained the native state. (The W42Q variant could not be oxidized efficiently due to extensive aggregation during the oxidizing treatment as shown in Fig. S5*C*.) Differential scanning fluorometry experiments revealed that all variants capable of forming the 108–SS–110 bond had decreased apparent T_m values upon oxidation relative to their reduced state (Fig. 6*A*). These decreases were not observed in constructs lacking either Cys^{108} or Cys^{110} but were present in all other cases. The conformational strain disappeared upon mild reduction, indicating that it was not due to any irreversible oxidative damage, such as Met or Trp oxidation (Fig. 6*B*). The average downshift in DSF T_m attributable to the 108–SS–110 bond was 5.4 °C with a standard deviation of 1.8 °C.

We next examined whether the conformational strain is global or confined to the C-terminal domain, which contains the disulfide. Differential scanning fluorometry assumes that the reporter fluorophore, in this case SYPRO Orange, binds to all relevant molten-globule states. However, DSF measurements conducted on the W42Q mutant (Fig. 6*C*) revealed only one melting transition, rather than the two transitions previously reported for this mutant by calorimetry, guanidinium denaturation, and intrinsic fluorescence (32, 68, 70, 71). The temperature of the transition was above the previously measured T_m of the N-terminal domain of the W42Q protein and close to its C-terminal T_m. Thus, SYPRO Orange likely bound preferentially to the molten-globule state of the C-terminal domain rather than the N-terminal domain. This surprising observation may help explain why chaperones fail to recognize the partial unfolding of the N-terminal domain in aggregation-prone, cataract-associated variants of this protein (70, 83). Apparently, unfolding of the N-terminal domain did not form a sufficiently hydrophobic binding pocket. This may be due in part to some of the N-terminal domain's residues being sequestered upon partial unfolding by interaction with the C-terminal domain, for example as proposed in Serebryany *et al*. (32).

To confirm the effect of the disulfide strain by a complementary label-free measurement, we carried out differential scanning calorimetry experiments at pH 5 to inhibit any disulfide exchange, comparing stock, oxidized, and oxidized-and-then-reduced WT HγD as well as identically treated C18T/C41A/C78A triple mutant. The results are summarized in Table 1. The stock WT protein was destabilized only modestly (3–4 °C) at lower pH compared with the previous neutral-pH measurements (32). However, oxidation led to a downshift of ~10 °C in the melting transition of one domain in the WT and ~7 °C in the triple mutant, whereas the other melting transition remained unchanged in both cases (Fig. S6). We attribute the redox-dependent melting transition to the C-terminal domain because the redox-active Cys pair is located there. The fitted calorimetric enthalpies for the two domains (shown in Table 1) were consistent with this assignment. Although these calculated enthalpies may be subject to variations in protein concentration or to aggregation during the experiment, the overall pattern was clear: enthalpy of the C-terminal domain was significantly higher than that of the N-terminal domain in reduced samples but dropped to become nearly identical to it following 108–SS–110 formation. The oxidized-and-then-reduced samples yielded traces and melting transitions very similar to those of the never-oxidized samples, indicating that destabilization

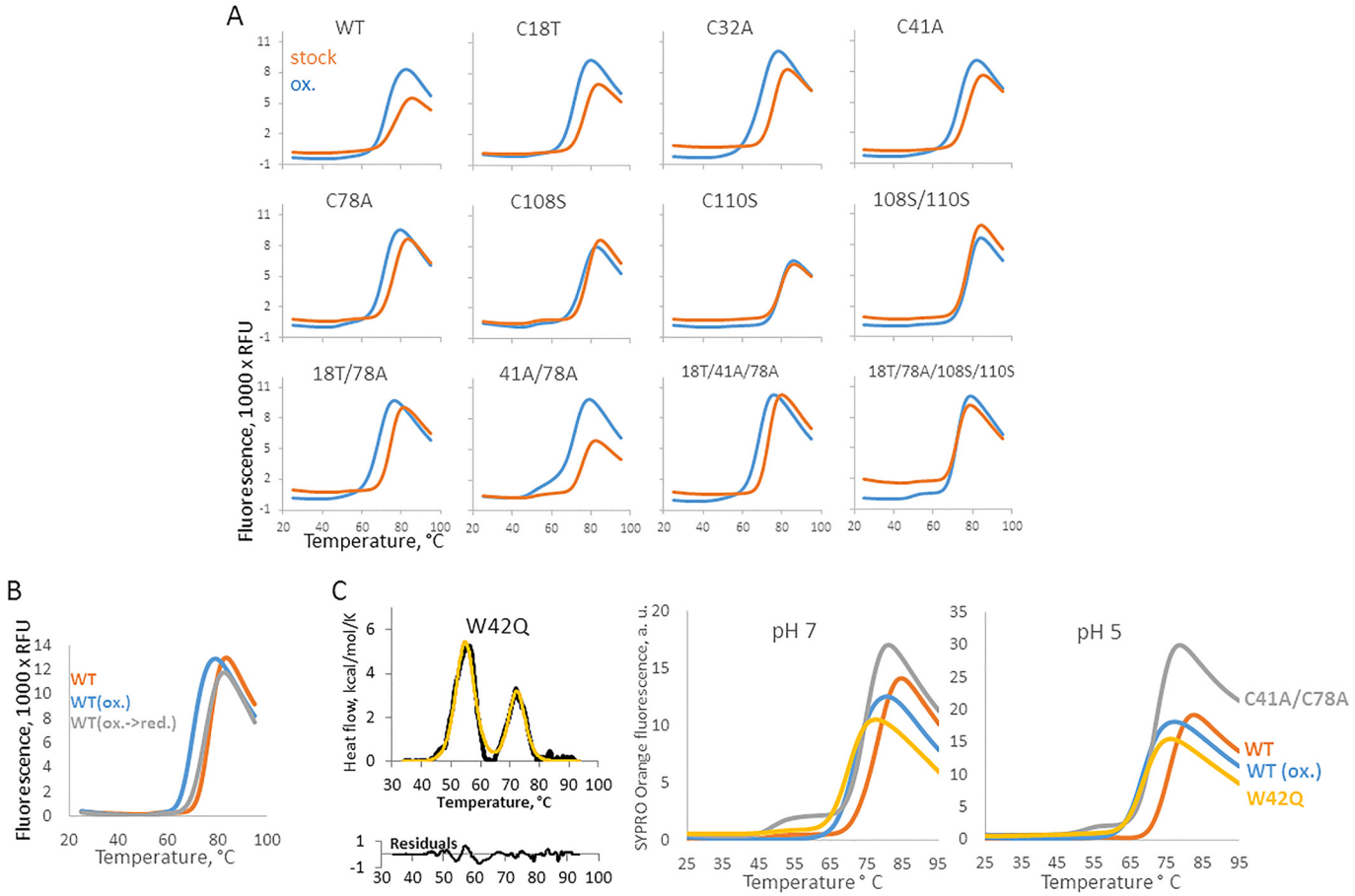

Figure 6. Formation of 108–SS–110 destabilizes the C-terminal domain. *A*, differential scanning fluorometry traces for oxidized (*orange*) and reduced (*blue*) WT and a panel of Cys mutants, detected by fluorescence of the hydrophobicity probe SYPRO Orange. All the oxidized samples capable of forming the 108–SS–110 disulfide showed a shift of the melting transition to lower temperatures, indicating that presence of the disulfide bond was destabilizing. No such shifts were observed for C108S, C110S, C108S/C110S, or C18T/C78A/C108S/C110S, all mutants that are not capable of forming the 108–SS–110 disulfide. *B*, the shift to lower T_m was reversible upon reduction, indicating that it was due to the 108–SS–110 bond and not irreversible oxidation. *C*, the shift was attributable to destabilization of the C-terminal domain alone. *Left*, the W42Q mutant is known to undergo two clear melting transitions, corresponding to the melting of the N- and C-terminal domains, respectively (data from Serebryany *et al.* (32)). *Right*, DSF traces of W42Q showed only a single melting transition at the same temperature as seen in the C41A/C78A double mutant as well as in WT(ox.) and only ~5 °C below that of WT. Thus, SYPRO Orange is a reporter of the melting of the C-terminal domain. A shoulder at ~50 °C in the oxidized C41A/C78A double mutant may be due to some misfolding or aggregation during the measurement. *RFU*, relative fluorescence units.

Table 1

Melting temperatures and enthalpies from fitting of WT and C18T/C41A/C78A HγD melting traces as a function of redox treatment

Melting traces were measured by differential scanning calorimetry at pH 5. Data are reported as the average ± 2 × S.E. of three replicates. N-td, N-terminal domain; C-td, C-terminal domain; red., reduced.

	Fitted T_m		Fitted ΔH	
	N-td	C-td	N-td	C-td
	℃		*kJ/mol*	
WT				
Stock	78.4 ± 0.1	81.8 ± 0.1	570 ± 18	878 ± 26
ox.	78.5 ± 0.1	71.5 ± 0.1	434 ± 30	467 ± 7
ox. → red.	77.3 ± 0.2	81.6 ± 0.2	438 ± 6	754 ± 15
C18T/C41A/C78A				
Stock	70.9 ± 0.8	73.5 ± 0.3	469 ± 42	791 ± 98
ox.	69.9 ± 1.4	66.2 ± 0.5	538 ± 74	435 ± 30
ox. → red.	70.5 ± 0.2	73.5 ± 0.1	438 ± 29	773 ± 29

due to oxidation was almost entirely redox-reversible and thus attributable to conformational strain induced by the 108–SS–110 disulfide.

The W130E oxidation-mimicking mutation in the C-terminal domain of HγD opens up a distinct nonnative, nonamyloid aggregation pathway, which is chaperone-suppressible but also partially redox-dependent (70). It is likely that the destabilization produced by the C-terminal mutation is in synergy with the conformational strain produced by the 108–SS–110 bond, and thus the disulfide indirectly promotes aggregation of this cataract-associated protein. Notably, UV irradiation, one of the best characterized causes of cataract, is known to damage Trp^{130} in HγD (67), and the UV-induced aggregation pathway requires oxidation (84). The N-terminal domain of HγD derives part of its stability from its interface with the C-terminal domain; disrupting this interface leads to N-terminal destabilization (85–88). The earliest detectable unfolding of the W42Q protein occurs at ~43 °C (32, 71), so if the 108–SS–110 bond forms in that variant and the resulting destabilization propagates to the domain interface, it may be sufficient to increase the population of aggregation-prone intermediates near 37 °C and in this way allosterically promote formation of the nonnative 32–SS–41 disulfide bond in the N-terminal domain that is required for aggregation. We have not found evidence of such an allosteric effect; however, a subtle allosteric effect on the N-terminal

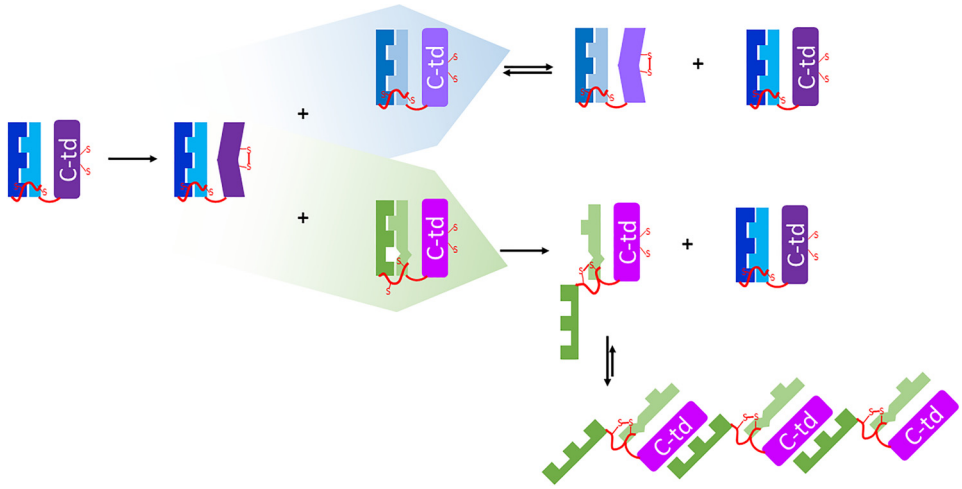

Figure 7. An illustration of the redox hot potato model of aggregation mediated by dynamic disulfide bonds. The WT, undamaged protein (*left*) may become oxidized, forming a conformationally strained and hence redox-active disulfide. This disulfide can then migrate to either a reduced WT or WT-like protein in a fully reversible reaction (*blue arrow*) or a damaged or mutated protein (here indicated by a perturbed native interaction in the N-terminal domain) (*green arrow*). In the latter case, it may migrate to a different location in the molecule, forming a conformationally relaxed and hence redox-inactive disulfide between Cys residues that are normally buried in the native state. This nonnative disulfide then traps a partially unfolded intermediate in a reaction that is essentially irreversible under mildly oxidizing conditions. The intermediate cannot revert to the native state and therefore partitions to aggregated structures. We have previously proposed a structural model for this aggregated state (32). *C-td*, C-terminal domain.

domain's dynamics near physiological temperature cannot be ruled out.

Discussion

The GSH redox buffer becomes depleted in the lens nucleus with age, whereas protein disulfide content increases (50, 58, 61–64). Other forms of protein oxidation, such as conversion of tryptophan to kynurenine, increase at the same time (64, 67, 89–91). We have described an unexpected synergy between these two modes of oxidative damage that results in rapid light-scattering aggregation due to the existence of a previously unrecognized oxidoreductase activity in human γD-crystallin. The oxidation-mimicking W42Q mutation, by partially destabilizing the N-terminal domain, enables 2 Cys residues that are distant and buried in the natively folded N-terminal domain to become solvent-exposed and transiently approach each other (32). We have now found that a redox-active disulfide in the C-terminal domain of the WT protein can then be transferred to these newly exposed N-terminal Cys residues in the mutant. The products of this bimolecular redox reaction are a soluble, fully reduced WT molecule and a W42Q molecule bearing a nonnative internal disulfide that locks its N-terminal domain in an aggregation-prone intermediate state (Fig. 7). The structure of this intermediate, and of the resulting aggregated state, has been proposed (32). The intermediate structure, detachment of the N-terminal β-hairpin, is consistent with that derived from single-molecule force spectroscopy (92), and evidence of the specific disulfide bond that traps this intermediate has been found in patient lenses and correlates strongly with age-onset cataract (58). It is worth noting that the latter two studies were carried out on unmutated proteins and that a large variety of congenital cataract-linked point mutations in the γ-crystallins (including the W42R mutation) cluster near this N-terminal hairpin (43). These observations raise the possibility that the W42Q mutation merely increases the population of a conformational intermediate that is already accessible, albeit extremely rare, in the WT protein and that other mutations and age-related post-translational modifications converge on the same aggregation-prone intermediate. In this model, the fact that the oxidized WT HγD does not aggregate on experimentally measurable timescales is simply due to the high kinetic and thermodynamic stability (93, 94) of its N-terminal domain.

The current study does not address the detailed mechanism by which HγD or its W42Q variant misfolds to form an aggregation-prone 32–SS–41 conformer. However, data in Fig. 3 suggest that the WT(ox.)/W42Q interaction is not limited to disulfide transfer. Specifically, W42Q at 50 μM aggregates much more rapidly with GSSG than with WT(ox.) (Fig. 3*A*), but W42Q at 20 μM aggregates much more rapidly with WT(ox.) than with GSSG (Fig. 3*B*). This surprising switch in relative efficacy of aggregation inducers suggests that WT(ox.) serves not only as an oxidant but also as an aggregation catalyst at low [W42Q]. We have previously hypothesized that an aggregation-promoting binding interaction between WT and W42Q may exist (71). Whether and how such an interaction affects misfolding and disulfide transfer to W42Q and other cataract-associated variants will be the subject of future research.

The specific model proposed here postulates transfer of the Cys^{108}-Cys^{110} disulfide from WT HγD to a nonnative N-terminal disulfide (Cys^{32}-Cys^{41}) of the W42Q mutant. Of the 6 Cys residues in HγD, five are well conserved among the γ-crystallins; Cys^{110} is the exception, being present in humans and chimpanzees but not in chicken, mouse, rat, or bovine γD sequences (95). Remarkably, however, each of those species has a Cys residue in position 110 in the closely related γC-crystallin, whereas human and chimpanzee versions of γC have Ser^{110} instead. Thermodynamically, HγD is more stable than HγC (43), and human lens proteomics has revealed that HγD persists longer than HγC, at least in its soluble form, becoming the most abundant soluble γ-crystallin by age ~55 (11). Thus, the apparent evolutionary switch of the Cys^{108}-Cys^{110} pair from γC to γD

might be a consequence of increased lifespan of the organism. At the same time, it is worth noting that at least one study identified other sequence-proximal disulfides in the γ-crystallins: the Cys^{78}-Cys^{79} bond in HγC and the Cys^{22}-Cys^{24} bond in HγS (74). It is not yet known whether these bonds are dynamic. Conversely, previous research also identified other nonnative internal disulfides in cataractous lenses, particularly in β-crystallins (57, 59), as well as one such bond in the lens-specific chaperone αA-crystallin, which appeared to diminish its chaperone activity as well as contribute to aggregation (60, 96). More recently, many disulfide bonds were discovered in noncrystallin proteins in the lens (97). It is possible that many of these long-lived lens proteins fall within the redox "hot potato" model we have proposed.

In redox-active proteins with a C*X*C or C*XX*C motif, the residues in the *X* positions are typically Gly, whose flexibility can best accommodate the conformational strain from the disulfide bond. In HγD, the *X* residue is Ser instead. Although this is the second most flexible amino acid after Gly (98), its presence is likely to produce a more strained disulfide with a higher redox potential than in the Cys-Gly-Cys disulfide isomerases. Nevertheless, a very recent reanalysis of proteomic data by Ramkumar *et al.* (99) revealed that 108–SS–110 disulfides in HγD are highly abundant in the human lens even prior to the onset of cataract.

What, then, is the possible fitness benefit of these sequence-proximal and likely redox-active disulfides? A possible explanation is that GSH levels become depleted in lens tissue during aging (50), and the lens core gradually becomes impermeable even to GSH generated in the lens cortex or present in vitreous humor (62), resulting in increased disulfide formation in lens cytoplasmic proteins (97). The γ-crystallins have always been thought of as purely structural proteins with no known biochemical function aside from their structural stability and optical properties (42, 43, 48). The search for the aggregation-promoting mechanism led us to a previously unrecognized oxidoreductase activity in WT HγD. Dynamic exchange of disulfide bonds among the protein molecules makes reduced and oxidized forms of HγD a redox couple. Given the high abundance of γ-crystallins, we speculate that they may constitute a protein-based redox buffer in the aging, GSH-depleted lens. If so, there is some evidence that this buffering capacity is enzymatically regulated *in vivo*. Early proteomic studies of the human eye lens indicated that Cys^{110} of HγD is partially (~30–70%) methylated (89). The significance of this observation was not known at the time but can now be interpreted as a likely regulation mechanism for the protein's oxidoreductase activity. Like Cys^{110} of HγD, Cys^{79} of HγC and Cys^{24} of HγS have also been found to be partially methylated *in vivo* (89, 100), suggesting a common physiological regulation mechanism. Cysteine methylation is an enzyme-catalyzed reaction *in vivo* (101). Our biochemical observations thus open up the possibility that an enzymatic pathway in the lens core actively regulates the redox buffering capacity of the crystallin proteome and may influence the age of onset of cataract.

Moreover, we have revealed a likely failure mode of such a protein-based redox homeostasis system: although sequence-proximal disulfides are kinetically favorable, nonnative disulfides are favored thermodynamically due to their propensity to aggregate. Destabilizing mutations or modifications of the HγD core, such as oxidation of Trp residues, may generate disulfide sinks analogous to the W42Q mutant. In general, we propose a redox hot potato mechanism in which polypeptides with lower kinetic stability (due to mutations or post-translational modifications) become trapped in aggregation-prone intermediate states and insolubilized as a consequence of accepting disulfides from more stable variants. The result is, essentially, a kinetic stability competition among protein variants competent for disulfide exchange with the conformational "weakest link" variant driven into an aggregated state upon receiving a disulfide. To participate in such a competition, the main features of the protein should be 1) the ability to exchange disulfides, or perhaps other reversible modifications, under physiologically relevant conditions and 2) a folding landscape that contains aggregation-prone intermediates that become more populated upon receiving the modification, in this case a disulfide bond, effectively serving as a sink for modified proteins. This process may have played a role in the evolution of the exceptional stability of the γ-crystallins or other long-lived proteins.

Experimental procedures

Site-directed mutagenesis

Site-directed mutagenesis was carried out using either the QuikChange II kit (Agilent, Santa Clara, CA) or the Q5 kit (New England Biolabs, Ipswich, MA) according to the manufacturers' instructions. Resulting plasmids, amplified in the XL-1 *Escherichia coli* strain (Agilent), were confirmed by sequencing and transformed into the BL21-RIL strain of *E. coli* for expression.

Protein expression and purification

Protein expression and purification were carried out largely as described (32, 71) with some modifications. Briefly, overnight starter cultures of BL21-RIL *E. coli* were inoculated in 10–40 ml of reconstituted SuperBroth medium (Teknova, Hollister, CA) supplemented with ampicillin and chloramphenicol. Expression cultures using the same medium in standard 2-liter flasks were inoculated at 1:100 from the starters and grown at 37 °C with shaking at 250 rpm for 6–8 h until reaching stationary phase (A_{600} ~ 2). Cultures were then chilled to 18 °C for 30 min and induced overnight at 18 °C by adding isopropyl 1-thio-β-D-galactopyranoside (Promega, Madison, WI) to 1 mM final concentration. Harvested cells were resuspended in the presence of protease inhibitors (Complete-mini, EDTA-free, Roche Applied Science) and stored at −70 °C until used.

Following lysis by sonication in the presence of DNase and lysozyme, purification was carried out by salting out with ammonium sulfate as described (71). The 50% ammonium sulfate supernatant was dialyzed at 4 °C overnight against 4 liters of sample buffer (10 mM ammonium acetate, 50 mM NaCl) to remove the ammonium sulfate. The dialysis step typically caused significant precipitation, attributable to peptidoglycan contaminants. Following centrifugation, these samples were then further scrubbed of lipids and peptidoglycans by passage through an anion-exchange column comprising two 5-ml Q-Sepharose columns (GE Healthcare) in tandem equilibrated in sample buffer. Crystallins eluted in the flow-through. The

ion-exchanged samples were concentrated using VivaSpin Turbo 5000 molecular weight cutoff centrifugal filters (Sartorius, Göttingen, Germany), loaded onto a Superdex 75 26 × 600-mm column (GE Healthcare), and separated at 2–3 ml/min flow rate at room temperature. Resulting fractions were collected and stored at 4 °C. SDS-PAGE (Criterion, Bio-Rad) was used to determine >95% purity of the samples. Proteins with the W42Q mutation were often found to have a minor degradation product at ~10 kDa in the gel, but its presence did not noticeably affect the overall aggregation behavior. Proteins were concentrated for storage at 4 °C to 100–500 μM; concentrations were determined by A_{280} using a NanoDrop 2000 instrument (Thermo Fisher, Waltham, MA).

In vitro oxidation

In vitro oxidation to form the 108–SS–110 disulfide bond was carried out by mixing 20 μM $CuSO_4$ and 60 μM phenanthroline (MilliporeSigma, Burlington, MA) in sample buffer at room temperature to chelate the copper and then adding the protein to 20 μM final concentration. This mixture, typically in 5–10-ml volume, was incubated at room temperature for 1–2 h in closed 15-ml conical tubes followed by addition of 1 mM EDTA and three rounds of dialysis through metal-free SpectraPor 7 dialysis membrane (Spectrum Labs, Breda, The Netherlands) at 4 °C against sample buffer for at least 3 h at a time (at least once overnight). The first round of dialysis included 1 mM EDTA in the sample buffer to fully chelate and remove the Cu^{2+} ions from the sample and avoid any copper-induced aggregation or oxidation during the subsequent experiments (102). To ensure that biochemical differences between the oxidized and reduced samples were due to reversible oxidation, *i.e.* disulfide formation, oxidized samples were subjected to mild reducing treatment, 1 mM DTT for 2 h at 37 °C, generating the oxidized → reduced controls.

Aggregation assay

Aggregation assays were carried out at 37 °C unless otherwise indicated using half-area clear polypropylene plates (Greiner Bio-One North America, Monroe, NC) in a PowerWave HT plate reader (BioTek, Winooski, VT) in a 100-μl volume without shaking. ~20% of the sample typically evaporated during the 3-h aggregation experiment. The resulting path length was ~0.5 cm, so the reported turbidity values are expected to be ~50% lower than in the typical 1-cm-pathlength spectrophotometer cuvette. Aggregation occurred on a comparable time scale in other reaction vessels, such as capped microcentrifuge or thermocycler tubes.

Differential scanning fluorometry

Differential scanning fluorometry was carried out using a 1:1 mixture of sample buffer and sodium phosphate (pH 7, 100 mM) buffer to maintain neutral pH during heating in 96-well format in a CFX96 RT-PCR instrument (Bio-Rad). 1× SYPRO Orange dye (Life Technologies) was added as the hydrophobicity probe; control (no-protein) samples were subtracted. The temperature ramp was 1 °C/min between 25 and 95 °C. Melting temperatures were defined as the minima (rounded to the nearest °C) of the derivative of the empirically fit sigmoid functions in the CFX Manager software (Bio-Rad).

Differential scanning calorimetry

Differential scanning calorimetry was carried out as reported previously (32) except in pH 5 buffer (20 mM ammonium acetate, 50 mM NaCl) to inhibit disulfide exchange during the measurement. Proteins were at 25 μM concentration. Samples were kept at 4 °C until immediately prior to analysis, which ran from 25 to 95 °C. Each melting trace was fitted to a sum of two two-state scaled models using NanoAnalyze software (TA Instruments, New Castle, DE).

PEGylation assays

PEGylation assays were carried out as follows. Samples were denatured for 5 min at 95 °C in pH 5 buffer (50 mM ammonium acetate) with 5% (w/v) SDS at [protein] of ~30 μM in a total volume of 10 μl per sample. Once cooled to room temperature, 10 μl of pH 8 buffer (100 mM sodium phosphate) was added to neutralize followed by 6 μl of 1 mM maleimide-conjugated PEG, M_r ~5000 (MilliporeSigma), and 4 μl of 4× NuPAGE SDS-PAGE gel-loading buffer (Thermo Fisher). The reaction mixtures were incubated at 50 °C for 2 h and then analyzed directly by SDS-PAGE with Coomassie stain (Thermo Fisher).

Isotopically resolved intact mass determination

Isotopically resolved intact mass determination was accomplished by electrospray ionization MS. The protein samples were analyzed on a Bruker Impact II q-TOF mass spectrometer equipped with an Agilent 1290 HPLC. The separation and desalting were performed on an Agilent PLRP-S column (1000 Å, 4.6 × 50 mm, 5 μm). Mobile phase A was 0.1% formic acid in water, and mobile phase B was acetonitrile with 0.1% formic acid. A constant flow rate of 0.300 ml/min was used. Ten microliters of the protein solution was injected and washed on the column for the first 2 min at 0% B, diverting nonretained materials to waste. The protein was then eluted using a linear gradient from 0% B to 100% B over 8 min. The mobile phase composition was maintained at 100% B for 1 min and then returned to 0% B over 0.1 min. The column was re-equilibrated to 0% B for the next 5.9 min. A plug of sodium formate was introduced at the end of the run to perform internal *m*/*z* calibration to obtain accurate *m*/*z* values. The data were analyzed using Bruker Compass DataAnalysis™ software (Version 4.3, Build 110.102.1532, 64 bit). The charge-state distribution for the protein produced by electrospray ionization was deconvoluted to neutral charge state using DataAnalysis implementation of the maximum entropy algorithm. Predicted isotope patterns were calculated at a resolving power of 50,000 and compared with isotopically resolved neutral mass spectra calculated using maximum entropy from the experimental charge-state distribution.

Disulfide mapping

Disulfide mapping was carried out using LC-MS/MS on an Orbitrap Fusion Lumos Tribrid mass spectrometer (Thermo Fisher) equipped with an EASY NanoLC 1000 pump (Thermo Fisher). Peptides were separated onto a 100-μm-inner diameter

microcapillary Kasil frit trapping column packed first with ~5 cm of C_{18} Reprosil resin (5 μm, 100 Å; Dr. Maisch GmbH, Ammerbuch-Entringen, Germany). Separation was achieved through applying a gradient from 5 to 27% acetonitrile in 0.1% formic acid over 90 min at 200 nl/min. Electrospray ionization was enabled through applying a voltage of 2 kV using a home-made electrode junction at the end of a Thermo Nano Viper 1200 75-μm × 550-mm column. The Fusion Lumos was operated in data-dependent mode for the MS methods. The MS survey scan was performed in the range of 395–1,800 m/z at a resolution of 6×10^4 with HCD fragmentation in the Fusion trap using a precursor isolation width window of 2 m/z. HCD collision energy was set at 32 V, isolation window was 3 Da with 30,000 Orbitrap, resolution for MS2 electron transfer and higher-energy collision dissociation scan was 200 ms, activation time was 10 ms, and automatic gain control was set to 50,000. Ions in a 10-ppm m/z window around ions selected for MS2 were excluded from further selection for fragmentation for 60 s.

WT(ox.) samples were treated with either chymotrypsin alone or the combination of trypsin and chymotrypsin. Samples were not carbamidomethylated or reduced; rather the pH of the digestion mixture was kept neutral or below at all times to minimize disulfide scrambling as in our previous report (32). W42Q aggregates were pelleted by centrifugation at 12,000 × g for 5–10 min, rinsed with 3 ml of sample buffer, and then resuspended in pH 5 ammonium acetate buffer. The suspension was centrifuged again, the supernatant was collected as the "pellet 1" fraction, and the remaining solid material was designated "pellet 2." Both were then denatured in SDS (the pellet 2 fraction could not be fully solubilized even in 5% SDS at 80 °C) and trypsinized using the suspension trapping (STrap) method (103) in spin column format (Protifi, Huntington, NY) with samples collected at 15, 45, and 90 min of incubation. Results were analyzed using Comet software and additionally verified by probability scores using PeptideProphet software with searches against the relevant subset of the CRAPome database of common contaminants (104), such as human keratins, within the Trans-Proteomic Pipeline. Only peptides with probability scores >0.95 were included in the analysis.

Top-down proteomics were used to confirm disulfide assignments using the same equipment as described above. WT(ox.) sample was codigested with chymotrypsin and Glu-C under incomplete-digestion conditions. Fragment MS1 spectra were deconvoluted by maximum entropy and assigned on the basis of their molecular weight as well as the weights of subfragments arising from in-source decay.

Author contributions—E. S. and E. I. S. conceptualization; E. S. and E. I. S. formal analysis; E. S., S. Y., S. A. T., and B. B. investigation; E. S., S. Y., S. A. T., and B. B. methodology; E. S., S. A. T., B. B., and E. I. S. writing-original draft; E. S. and E. I. S. writing-review and editing; B. B. data curation; E. I. S. supervision; E. I. S. funding acquisition.

Acknowledgments—We thank Prof. Jonathan A. King for mentorship and discussion at the early stages of this research. We thank Renee Robinson for technical assistance with MS.

References

1. Walsh, C. T., Garneau-Tsodikova, S., and Gatto, G. J., Jr. (2005) Protein posttranslational modifications: the chemistry of proteome diversifications. *Angew. Chem. Int. Ed. Engl.* **44,** 7342–7372 CrossRef Medline
2. Hornbeck, P. V., Kornhauser, J. M., Tkachev, S., Zhang, B., Skrzypek, E., Murray, B., Latham, V., and Sullivan, M. (2012) PhosphoSitePlus: a comprehensive resource for investigating the structure and function of experimentally determined post-translational modifications in man and mouse. *Nucleic Acids Res.* **40,** D261–D270 CrossRef Medline
3. Fuchs, S. M., Krajewski, K., Baker, R. W., Miller, V. L., and Strahl, B. D. (2011) Influence of combinatorial histone modifications on antibody and effector protein recognition. *Curr. Biol.* **21,** 53–58 CrossRef Medline
4. Bah, A., and Forman-Kay, J. D. (2016) Modulation of intrinsically disordered protein function by post-translational modifications. *J. Biol. Chem.* **291,** 6696–6705 CrossRef Medline
5. Deis, L. N., Pemble, C. W., 4th, Qi, Y., Hagarman, A., Richardson, D. C., Richardson, J. S., and Oas, T. G. (2014) Multiscale conformational heterogeneity in staphylococcal protein a: possible determinant of functional plasticity. *Structure* **22,** 1467–1477 CrossRef Medline
6. Xin, F., and Radivojac, P. (2012) Post-translational modifications induce significant yet not extreme changes to protein structure. *Bioinformatics* **28,** 2905–2913 CrossRef Medline
7. Lu, H. P., Xun, L., and Xie, X. S. (1998) Single-molecule enzymatic dynamics. *Science* **282,** 1877–1882 CrossRef Medline
8. Murzin, A. G. (2008) Biochemistry. Metamorphic proteins. *Science* **320,** 1725–1726 CrossRef Medline
9. Truscott, R. J. W., Schey, K. L., and Friedrich, M. G. (2016) Old proteins in man: a field in its infancy. *Trends Biochem. Sci.* **41,** 654–664 CrossRef Medline
10. de Graff, A. M., Hazoglou, M. J., and Dill, K. A. (2016) Highly charged proteins: the Achilles' heel of aging proteomes. *Structure* **24,** 329–336 CrossRef Medline
11. Ma, Z., Hanson, S. R., Lampi, K. J., David, L. L., Smith, D. L., and Smith, J. B. (1998) Age-related changes in human lens crystallins identified by HPLC and mass spectrometry. *Exp. Eye Res.* **67,** 21–30 CrossRef Medline
12. Horwich, A. (2002) Protein aggregation in disease: a role for folding intermediates forming specific multimeric interactions. *J. Clin. Investig.* **110,** 1221–1232 CrossRef Medline
13. Bartlett, A. I., and Radford, S. E. (2009) An expanding arsenal of experimental methods yields an explosion of insights into protein folding mechanisms. *Nat. Struct. Mol. Biol.* **16,** 582–588 CrossRef Medline
14. Chiti, F., and Dobson, C. M. (2009) Amyloid formation by globular proteins under native conditions. *Nat. Chem. Biol.* **5,** 15–22 CrossRef Medline
15. Wang, Y., Papaleo, E., and Lindorff-Larsen, K. (2016) Mapping transiently formed and sparsely populated conformations on a complex energy landscape. *Elife* **5,** e17505 CrossRef Medline
16. Forman-Kay, J. D., and Mittag, T. (2013) From sequence and forces to structure, function, and evolution of intrinsically disordered proteins. *Structure* **21,** 1492–1499 CrossRef Medline
17. Aguzzi, A., and Calella, A. M. (2009) Prions: protein aggregation and infectious diseases. *Physiol. Rev.* **89,** 1105–1152 CrossRef Medline
18. Grad, L. I., and Cashman, N. R. (2014) Prion-like activity of Cu/Zn superoxide dismutase: implications for amyotrophic lateral sclerosis. *Prion* **8,** 33–41 CrossRef Medline
19. Karamanos, T. K., Kalverda, A. P., Thompson, G. S., and Radford, S. E. (2014) Visualization of transient protein-protein interactions that promote or inhibit amyloid assembly. *Mol. Cell* **55,** 214–226 CrossRef Medline
20. Tessier, P. M., and Lindquist, S. (2007) Prion recognition elements govern nucleation, strain specificity and species barriers. *Nature* **447,** 556–561 CrossRef Medline
21. Trivedi, M. V., Laurence, J. S., and Siahaan, T. J. (2009) The role of thiols and disulfides on protein stability. *Curr. Protein Pept. Sci.* **10,** 614–625 CrossRef Medline
22. Thornton, J. M. (1981) Disulfide bridges in globular proteins. *J. Mol. Biol.* **151,** 261–287 CrossRef Medline

23. Creighton, T. E. (1988) Disulphide bonds and protein stability. *BioEssays* **8,** 57–63 CrossRef Medline
24. Fass, D., and Thorpe, C. (2018) Chemistry and enzymology of disulfide cross-linking in proteins. *Chem. Rev.* **118,** 1169–1198 CrossRef Medline
25. Sevier, C. S., and Kaiser, C. A. (2002) Formation and transfer of disulphide bonds in living cells. *Nat. Rev. Mol. Cell Biol.* **3,** 836–847 CrossRef Medline
26. Woycechowsky, K. J., and Raines, R. T. (2000) Native disulfide bond formation in proteins. *Curr. Opin. Chem. Biol.* **4,** 533–539 CrossRef Medline
27. Go, Y. M., Chandler, J. D., and Jones, D. P. (2015) The cysteine proteome. *Free Radic. Biol. Med.* **84,** 227–245 CrossRef Medline
28. Hua, Q. X., Jia, W., Frank, B. H., Phillips, N. F., and Weiss, M. A. (2002) A protein caught in a kinetic trap: structures and stabilities of insulin disulfide isomers. *Biochemistry* **41,** 14700–14715 CrossRef Medline
29. Chang, J. Y., Li, L., and Lai, P. H. (2001) A major kinetic trap for the oxidative folding of human epidermal growth factor. *J. Biol. Chem.* **276,** 4845–4852 CrossRef Medline
30. Arolas, J. L., Aviles, F. X., Chang, J. Y., and Ventura, S. (2006) Folding of small disulfide-rich proteins: clarifying the puzzle. *Trends Biochem. Sci.* **31,** 292–301 CrossRef Medline
31. Toichi, K., Yamanaka, K., and Furukawa, Y. (2013) Disulfide scrambling describes the oligomer formation of superoxide dismutase (SOD1) proteins in the familial form of amyotrophic lateral sclerosis. *J. Biol. Chem.* **288,** 4970–4980 CrossRef Medline
32. Serebryany, E., Woodard, J. C., Adkar, B. V., Shabab, M., King, J. A., and Shakhnovich, E. I. (2016) An internal disulfide locks a misfolded aggregation-prone intermediate in cataract-linked mutants of human γD-crystallin. *J. Biol. Chem.* **291,** 19172–19183 CrossRef Medline
33. Smith, D. P., and Radford, S. E. (2001) Role of the single disulphide bond of β_2-microglobulin in amyloidosis *in vitro*. *Protein Sci.* **10,** 1775–1784 CrossRef Medline
34. Chen, Y., and Dokholyan, N. V. (2005) A single disulfide bond differentiates aggregation pathways of β2-microglobulin. *J. Mol. Biol.* **354,** 473–482 CrossRef Medline
35. Connors, L. H., Jiang, Y., Budnik, M., Théberge, R., Prokaeva, T., Bodi, K. L., Seldin, D. C., Costello, C. E., and Skinner, M. (2007) Heterogeneity in primary structure, post-translational modifications, and germline gene usage of nine full-length amyloidogenic kappa1 immunoglobulin light chains. *Biochemistry* **46,** 14259–14271 CrossRef Medline
36. Ronzoni, R., Berardelli, R., Medicina, D., Sitia, R., Gooptu, B., and Fra, A. M. (2016) Aberrant disulphide bonding contributes to the ER retention of α1-antitrypsin deficiency variants. *Hum. Mol. Genet.* **25,** 642–650 CrossRef Medline
37. Oka, O. B., Yeoh, H. Y., and Bulleid, N. J. (2015) Thiol-disulfide exchange between the PDI family of oxidoreductases negates the requirement for an oxidase or reductase for each enzyme. *Biochem. J.* **469,** 279–288 CrossRef Medline
38. Cook, K. M., and Hogg, P. J. (2013) Post-translational control of protein function by disulfide bond cleavage. *Antioxid. Redox Signal.* **18,** 1987–2015 CrossRef Medline
39. Sarsour, E. H., Kumar, M. G., Chaudhuri, L., Kalen, A. L., and Goswami, P. C. (2009) Redox control of the cell cycle in health and disease. *Antioxid. Redox Signal.* **11,** 2985–3011 CrossRef Medline
40. Jones, D. P. (2010) Redox sensing: orthogonal control in cell cycle and apoptosis signalling. *J. Intern. Med.* **268,** 432–448 CrossRef Medline
41. Banerjee, R. (2012) Redox outside the box: linking extracellular redox remodeling with intracellular redox metabolism. *J. Biol. Chem.* **287,** 4397–4402 CrossRef Medline
42. Moreau, K. L., and King, J. A. (2012) Protein misfolding and aggregation in cataract disease and prospects for prevention. *Trends Mol. Med.* **18,** 273–282 CrossRef Medline
43. Serebryany, E., and King, J. A. (2014) The βγ-crystallins: native state stability and pathways to aggregation. *Prog. Biophys. Mol. Biol.* **115,** 32–41 CrossRef Medline
44. Hains, P. G., and Truscott, R. J. (2007) Post-translational modifications in the nuclear region of young, aged, and cataract human lenses. *J. Proteome Res.* **6,** 3935–3943 CrossRef Medline
45. Hains, P. G., and Truscott, R. J. (2008) Proteomic analysis of the oxidation of cysteine residues in human age-related nuclear cataract lenses. *Biochim. Biophys. Acta* **1784,** 1959–1964 CrossRef Medline
46. Lampi, K. J., Wilmarth, P. A., Murray, M. R., and David, L. L. (2014) Lens β-crystallins: the role of deamidation and related modifications in aging and cataract. *Prog. Biophys. Mol. Biol.* **115,** 21–31 CrossRef Medline
47. Hoehenwarter, W., Klose, J., and Jungblut, P. R. (2006) Eye lens proteomics. *Amino Acids* **30,** 369–389 CrossRef Medline
48. Bloemendal, H., de Jong, W., Jaenicke, R., Lubsen, N. H., Slingsby, C., and Tardieu, A. (2004) Ageing and vision: structure, stability and function of lens crystallins. *Prog. Biophys. Mol. Biol.* **86,** 407–485 CrossRef Medline
49. Wride, M. A. (2011) Lens fibre cell differentiation and organelle loss: many paths lead to clarity. *Philos. Trans. R. Soc. Lond. B Biol. Sci.* **366,** 1219–1233 CrossRef Medline
50. Friedburg, D., and Manthey, K. F. (1973) Glutathione and NADP linked enzymes in human senile cataract. *Exp. Eye Res.* **15,** 173–177 CrossRef Medline
51. Michael, R., and Bron, A. J. (2011) The ageing lens and cataract: a model of normal and pathological ageing. *Philos. Trans. R. Soc. Lond. B Biol. Sci.* **366,** 1278–1292 CrossRef Medline
52. Shang, F., and Taylor, A. (2004) Function of the ubiquitin proteolytic pathway in the eye. *Exp. Eye Res.* **78,** 1–14 CrossRef Medline
53. Spector, A., and Roy, D. (1978) Disulfide-linked high molecular-weight protein associated with human cataract. *Proc. Natl. Acad. Sci. U.S.A.* **75,** 3244–3248 CrossRef Medline
54. Giblin, F. J., Padgaonkar, V. A., Leverenz, V. R., Lin, L. R., Lou, M. F., Unakar, N. J., Dang, L., Dickerson, J. E., Jr., and Reddy, V. N. (1995) Nuclear light-scattering, disulfide formation, and membrane damage in lenses of older guinea-pigs treated with hyperbaric oxygen. *Exp. Eye Res.* **60,** 219–235 CrossRef Medline
55. Ozaki, Y., Mizuno, A., Itoh, K., and Iriyama, K. (1987) Inter- and intramolecular disulfide bond formation and related structural changes in the lens proteins. A Raman spectroscopic study *in vivo* of lens aging. *J. Biol. Chem.* **262,** 15545–15551 Medline
56. Yu, N. T., DeNagel, D. C., Pruett, P. L., and Kuck, J. F., Jr. (1985) Disulfide bond formation in the eye lens. *Proc. Natl. Acad. Sci. U.S.A.* **82,** 7965–7968 CrossRef Medline
57. Takemoto, L. J. (1997) Disulfide bond formation of cysteine-37 and cysteine-66 of βB2 crystallin during cataractogenesis of the human lens. *Exp. Eye Res.* **64,** 609–614 CrossRef Medline
58. Fan, X., Zhou, S., Wang, B., Hom, G., Guo, M., Li, B., Yang, J., Vaysburg, D., and Monnier, V. M. (2015) Evidence of highly conserved β-crystallin disulfidome that can be mimicked by *in vitro* oxidation in age-related human cataract and glutathione depleted mouse lens. *Mol. Cell. Proteomics* **14,** 3211–3223 CrossRef Medline
59. Takemoto, L. J. (1997) βA3/A1 crystallin from human cataractous lens contains an intramolecular disulfide bond. *Curr. Eye Res.* **16,** 719–724 CrossRef Medline
60. Cherian-Shaw, M., Smith, J. B., Jiang, X. Y., and Abraham, E. C. (1999) Intrapolypeptide disulfides in human αA-crystallin and their effect on chaperone-like function. *Mol. Cell. Biochem.* **199,** 163–167 CrossRef Medline
61. Lou, M. F., and Dickerson, J. E. (1992) Protein thiol mixed disulfides in human lens. *Exp. Eye Res.* **55,** 889–896 CrossRef Medline
62. Sweeney, M. H., and Truscott, R. J. (1998) An impediment to glutathione diffusion in older normal human lenses: a possible precondition for nuclear cataract. *Exp. Eye Res.* **67,** 587–595 CrossRef Medline
63. Lou, M. F. (2003) Redox regulation in the lens. *Prog. Retin. Eye Res.* **22,** 657–682 CrossRef Medline
64. Boscia, F., Grattagliano, I., Vendemiale, G., Micelli-Ferrari, T., and Altomare, E. (2000) Protein oxidation and lens opacity in humans. *Invest. Ophthalmol. Vis. Sci.* **41,** 2461–2465 Medline
65. Siezen, R. J., Thomson, J. A., Kaplan, E. D., and Benedek, G. B. (1987) Human lens γ-crystallins—isolation, identification, and characterization of the expressed gene products. *Proc. Natl. Acad. Sci. U.S.A.* **84,** 6088–6092 CrossRef Medline
66. Su, S., Liu, P., Zhang, H., Li, Z., Song, Z., Zhang, L., and Chen, S. (2011) Proteomic analysis of human age-related nuclear cataracts and normal

lens nuclei. *Invest. Ophthalmol. Vis. Sci.* **52,** 4182–4191 CrossRef Medline
67. Moran, S. D., Zhang, T. O., Decatur, S. M., and Zanni, M. T. (2013) Amyloid fiber formation in human γD-Crystallin induced by UV-B photodamage. *Biochemistry* **52,** 6169–6181 CrossRef Medline
68. Ji, F., Jung, J., Koharudin, L. M., and Gronenborn, A. M. (2013) The human W42R γD-crystallin mutant structure provides a link between congenital and age-related cataracts. *J. Biol. Chem.* **288,** 99–109 CrossRef Medline
69. Wang, B., Yu, C., Xi, Y. B., Cai, H. C., Wang, J., Zhou, S., Zhou, S., Wu, Y., Yan, Y. B., Ma, X., and Xie, L. (2011) A novel CRYGD mutation (p.Trp43Arg) causing autosomal dominant congenital cataract in a Chinese family. *Hum. Mutat.* **32,** E1939–E1947 CrossRef Medline
70. Serebryany, E., Takata, T., Erickson, E., Schafheimer, N., Wang, Y., and King, J. A. (2016) Aggregation of Trp > Glu point mutants of human γ-D crystallin provides a model for hereditary or UV-induced cataract. *Protein Sci.* **25,** 1115–1128 CrossRef Medline
71. Serebryany, E., and King, J. A. (2015) Wild-type human γD-crystallin promotes aggregation of its oxidation-mimicking, misfolding-prone W42Q mutant. *J. Biol. Chem.* **290,** 11491–11503 CrossRef Medline
72. Kobashi, K. (1968) Catalytic oxidation of sulfhydryl groups by o-phenanthroline copper complex. *Biochim. Biophys. Acta* **158,** 239–245 CrossRef Medline
73. Careaga, C. L., and Falke, J. J. (1992) Thermal motions of surface α-helices in the D-galactose chemosensory receptor. Detection by disulfide trapping. *J. Mol. Biol.* **226,** 1219–1235 CrossRef Medline
74. Hanson, S. R., Smith, D. L., and Smith, J. B. (1998) Deamidation and disulfide bonding in human lens γ-crystallins. *Exp. Eye Res.* **67,** 301–312 CrossRef Medline
75. Woycechowsky, K. J., and Raines, R. T. (2003) The CXC motif: a functional mimic of protein disulfide isomerase. *Biochemistry* **42,** 5387–5394 CrossRef Medline
76. Lu, J., and Deutsch, C. (2001) Pegylation: a method for assessing topological accessibilities in Kv1.3. *Biochemistry* **40,** 13288–13301 CrossRef Medline
77. Basilio, D., Noack, K., Picollo, A., and Accardi, A. (2014) Conformational changes required for H^+/Cl^- exchange mediated by a CLC transporter. *Nat. Struct. Mol. Biol.* **21,** 456–463 CrossRef Medline
78. Goodson, R. J., and Katre, N. V. (1990) Site-directed pegylation of recombinant interleukin-2 at its glycosylation site. *Biotechnology* **8,** 343–346 Medline
79. Robertson, A. D., and Murphy, K. P. (1997) Protein structure and the energetics of protein stability. *Chem. Rev.* **97,** 1251–1268 CrossRef Medline
80. Derewenda, U., Boczek, T., Gorres, K. L., Yu, M., Hung, L. W., Cooper, D., Joachimiak, A., Raines, R. T., and Derewenda, Z. S. (2009) Structure and function of *Bacillus subtilis* YphP, a prokaryotic disulfide isomerase with a CXC catalytic motif. *Biochemistry* **48,** 8664–8671 CrossRef Medline
81. Jakob, U., Muse, W., Eser, M., and Bardwell, J. C. (1999) Chaperone activity with a redox switch. *Cell* **96,** 341–352 CrossRef Medline
82. Basak, A., Bateman, O., Slingsby, C., Pande, A., Asherie, N., Ogun, O., Benedek, G. B., and Pande, J. (2003) High-resolution X-ray crystal structures of human γD crystallin (1.25 Å) and the R58H mutant (1.15 Å) associated with aculeiform cataract. *J. Mol. Biol.* **328,** 1137–1147 CrossRef Medline
83. Moreau, K. L., and King, J. A. (2012) Cataract-causing defect of a mutant γ-crystallin proceeds through an aggregation pathway which bypasses recognition by the α-crystallin chaperone. *PLoS One* **7,** e37256 CrossRef Medline
84. Schafheimer, N., and King, J. (2013) Tryptophan cluster protects human γD-crystallin from ultraviolet radiation-induced photoaggregation *in vitro*. *Photochem. Photobiol.* **89,** 1106–1115 CrossRef Medline
85. Moreau, K. L., and King, J. (2009) Hydrophobic core mutations associated with cataract development in mice destabilize human γD-crystallin. *J. Biol. Chem.* **284,** 33285–33295 CrossRef Medline
86. Flaugh, S. L., Kosinski-Collins, M. S., and King, J. (2005) Interdomain side-chain interactions in human γD crystallin influencing folding and stability. *Protein Sci.* **14,** 2030–2043 CrossRef Medline
87. Flaugh, S. L., Kosinski-Collins, M. S., and King, J. (2005) Contributions of hydrophobic domain interface interactions to the folding and stability of human γD-crystallin. *Protein Sci.* **14,** 569–581 CrossRef Medline
88. Mills, I. A., Flaugh, S. L., Kosinski-Collins, M. S., and King, J. A. (2007) Folding and stability of the isolated Greek key domains of the long-lived human lens proteins γD-crystallin and γS-crystallin. *Protein Sci.* **16,** 2427–2444 CrossRef Medline
89. Lapko, V. N., Smith, D. L., and Smith, J. B. (2003) Methylation and carbamylation of human γ-crystallins. *Protein Sci.* **12,** 1762–1774 CrossRef Medline
90. McDermott, M., Chiesa, R., Roberts, J. E., and Dillon, J. (1991) Photooxidation of specific residues in α-crystallin polypeptides. *Biochemistry* **30,** 8653–8660 CrossRef Medline
91. Finley, E. L., Dillon, J., Crouch, R. K., and Schey, K. L. (1998) Identification of tryptophan oxidation products in bovine α-crystallin. *Protein Sci.* **7,** 2391–2397 CrossRef Medline
92. Garcia-Manyes, S., Giganti, D., Badilla, C. L., Lezamiz, A., Perales-Calvo, J., Beedle, A. E., and Fernández, J. M. (2016) Single-molecule force spectroscopy predicts a misfolded, domain-swapped conformation in human γD-crystallin protein. *J. Biol. Chem.* **291,** 4226–4235 CrossRef Medline
93. Kosinski-Collins, M. S., and King, J. (2003) *In vitro* unfolding, refolding, and polymerization of human γD crystallin, a protein involved in cataract formation. *Protein Sci.* **12,** 480–490 CrossRef Medline
94. Flaugh, S. L., Mills, I. A., and King, J. (2006) Glutamine deamidation destabilizes human γD-crystallin and lowers the kinetic barrier to unfolding. *J. Biol. Chem.* **281,** 30782–30793 CrossRef Medline
95. Kong, F., and King, J. (2011) Contributions of aromatic pairs to the folding and stability of long-lived human γD-crystallin. *Protein Sci.* **20,** 513–528 CrossRef Medline
96. Takemoto, L. J. (1996) Oxidation of cysteine residues from α-A crystallin during cataractogenesis of the human lens. *Biochem. Biophys. Res. Commun.* **223,** 216–220 CrossRef Medline
97. Wang, B., Hom, G., Zhou, S., Guo, M., Li, B., Yang, J., Monnier, V. M., and Fan, X. (2017) The oxidized thiol proteome in aging and cataractous mouse and human lens revealed by ICAT labeling. *Aging Cell* **16,** 244–261 CrossRef Medline
98. Huang, F., and Nau, W. M. (2003) A conformational flexibility scale for amino acids in peptides. *Angew. Chem. Int. Ed. Engl.* **42,** 2269–2272 CrossRef Medline
99. Ramkumar, S., Fan, X., Wang, B., Yang, S., and Monnier, V. M. (2018) Reactive cysteine residues in the oxidative dimerization and Cu^{2+} induced aggregation of human γD-crystallin: implications for age-related cataract. *Biochim. Biophys. Acta Mol. Basis Dis.* **1864,** 3595–3604 CrossRef Medline
100. Lapko, V. N., Smith, D. L., and Smith, J. B. (2002) S-Methylated cysteines in human lens γS-crystallins. *Biochemistry* **41,** 14645–14651 CrossRef Medline
101. Clarke, S. G. (2013) Protein methylation at the surface and buried deep: thinking outside the histone box. *Trends Biochem. Sci.* **38,** 243–252 CrossRef Medline
102. Quintanar, L., Domínguez-Calva, J. A., Serebryany, E., Rivillas-Acevedo, L., Haase-Pettingell, C., Amero, C., and King, J. A. (2016) Copper and zinc ions specifically promote nonamyloid aggregation of the highly stable human γ-D crystallin. *ACS Chem. Biol.* **11,** 263–272 CrossRef Medline
103. Zougman, A., Selby, P. J., and Banks, R. E. (2014) Suspension trapping (STrap) sample preparation method for bottom-up proteomics analysis. *Proteomics* **14,** 1006–1010 CrossRef Medline
104. Mellacheruvu, D., Wright, Z., Couzens, A. L., Lambert, J. P., St-Denis, N. A., Li, T., Miteva, Y. V., Hauri, S., Sardiu, M. E., Low, T. Y., Halim, V. A., Bagshaw, R. D., Hubner, N. C., Al-Hakim, A., Bouchard, A., *et al.* (2013) The CRAPome: a contaminant repository for affinity purification-mass spectrometry data. *Nat. Methods* **10,** 730–736 CrossRef Medline